JACS
JOURNAL OF THE AMERICAN CHEMICAL SOCIETY
Article
pubs.acs.org/JACS

Metal–Organic Microstructures: From Rectangular to Stellated and Interpenetrating Polyhedra

Sreejith Shankar,[†] Renata Balgley,[†] Michal Lahav,[†] Sidney R. Cohen,[‡] Ronit Popovitz-Biro,[‡] and Milko E. van der Boom*[,†]

[†]Department of Organic Chemistry and [‡]Department of Chemical Research Support, Weizmann Institute of Science, Rehovot 7610001, Israel

Supporting Information

ABSTRACT: Despite the tremendous progress made in the design of supramolecular and inorganic materials, it still remains a great challenge to obtain uniform structures with tailored size and shape. Metal–organic frameworks and infinite coordination polymers are examples of rapidly emerging materials with useful properties, yet limited morphological control. In this paper, we report the solvothermal synthesis of diverse metal–organic (sub)-microstructures with a high degree of uniformity. The porous and thermally robust monodisperse crystalline solids consist of tetrahedral polypyridyl ligands and nickel or copper ions. Our bottom-up approach demonstrates the direct assembly of these materials without the addition of any surfactants or modulators. Reaction parameters in combination with molecular structure encoding are the keys to size-shape control and structural uniformity of our metal–organic materials.

INTRODUCTION

Structural uniformity is a prerequisite for many real-world applications that involve oriented fabrication of various materials, often in size-confined regimes.[1] At the same time, structural diversity can lead to control of desired physical and chemical properties.[2−6] Molecular self-assembly allows the construction of composites with unique properties and structure. Size and shape confined synthesis of composites is advantageous for the resulting intrinsic and complex multifunctionalities, opening the opportunity to address properties of both the individual components, and those of the composite as a whole.[7] Previous studies have shown that solvents play a significant role in the formation of MOFs.[8−11] For instance, colloidal MOF particles were reported by Granick that are monodisperse in size and shape, while the geometrical shape was controlled by the cosolvents.[8]

In this work, we report on the structural uniformity and diversity of metal–organic frameworks (MOFs). Due to their unique, often porous structures and special properties achieved through synthetic tunability, MOFs have been actively studied over the last few decades.[12−14] However, control over their structure at the nano and micro levels is still limited and difficult to achieve.[15−21] Many variables (e.g., anions, solvents, electronic configuration) play a key role in the formation of geometrically well-defined and uniform shapes. Thus far, the shapes of MOFs are mainly limited to polyhedra.[16]

RESULTS AND DISCUSSION

We introduce here the assembly of a series of three-dimensional (3D) (sub)microstructured MOFs with a narrow size distribution without the need for a modulator to define the crystal morphology. Diverse structures are demonstrated in this study ranging from elongated hexagons and rectangular prisms to stellated and interpenetrating polyhedra by systematically varying the (i) metal center, (ii) anion, (iii) organic ligand, and (iv) reaction conditions (i.e., solvent, temperature, aerobic vs anaerobic). For instance, the use of Ni(II) salts result in distinct polyhedral morphologies as opposed to Cu(II) precursors that form interpenetrating and/or stellated polyhedra. Such metal–organic structures are highly uncommon.[5] Kitagawa et al. showed recently how the concentration of a modulator (*n*-dodecanoic acid or lauric acid) can be used to control the morphology of MOFs.[22] The uniformity in shape and size of our materials is attained via solvothermal synthesis without the use of surfactants or external modulators.[16,18,20,21,23−26] Follow-up electron microscopy studies of the formation of our MOFs revealed a complex sequence of reactions. For the Ni-based MOFs two types of growth processes were observed involving nucleation and polishing, whereas fusion processes play a dominant role in the formation of the Cu-based MOFs.

To form our metal–organic microstructures, ligand–metal–anion combinations are needed that form robust and extended 3D networks by interconnected tetrahedral nodes allowing the generation of diamondoid networks.[27] Such networks might have exceptionally high permanent microporosities and/or channels with incorporation of solvent molecules to stabilize the microstructures. Therefore, we used two organic ligands **L1**[28] and **L2**[29] (Figure 1) and commercially available salts of Ni(II) and Cu(II). These tetrahedral ligands are rigid, possess T_d symmetry, and four metal ion binding sites. This combination ensures the formation of robust, porous, and extended 3D networks.[30−32] Ni(II) and Cu(II) salts have a high affinity for pyridyl ligands,[33,34] nevertheless the metal–N bond

Received: September 19, 2014
Published: December 3, 2014

DOI: 10.1021/ja509428a
J. Am. Chem. Soc. 2015, 137, 226−231

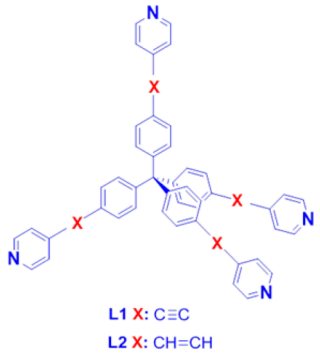

Figure 1. Molecular structure of the ligands.

strength allows for the rearrangement of kinetic structures into thermodynamic products to occur at elevated temperatures.[35] The scope of this work is demonstrated by the use of two metals that have different coordination requirements. In addition, the dominant role of the anions in the formation of our microstructures has been demonstrated.

In a typical experiment, a DMF solution of the metal salt was mixed with a chloroform solution of 0.5 or 1 equiv of **L1** or **L2** (Figure 1) and heated in a glass pressure tube at 105 °C with the exclusion of light. After 4−5 days the reaction mixture was gradually cooled over 9−10 h, and the microstructures were collected quantitatively by centrifugation. The crystalline microstructures have been characterized by electron microscope (EM) analysis, X-ray diffraction (XRD), and atomic force microscope (AFM). Information at the molecular level has been obtained by infrared (IR) spectroscopy, magnetic measurements, and gas adsorption. The nickel structures have also been tested for their thermal stability.

SEM and TEM imaging revealed that the combinations of $NiCl_2$ and **L1** or $NiBr_2$ and **L2** in a 2:1 ratio, respectively, yield monodispersed structures (**NiClL1** (Figures 2 and 5A) and **NiBrL2** (Figures 3 and 5C). Although both MOFs have regular hexagonal morphologies, **NiClL1** forms distinctly elongated hexagons that can also be observed by optical microscopy (Figure S1, inset). These observations demonstrate that minor

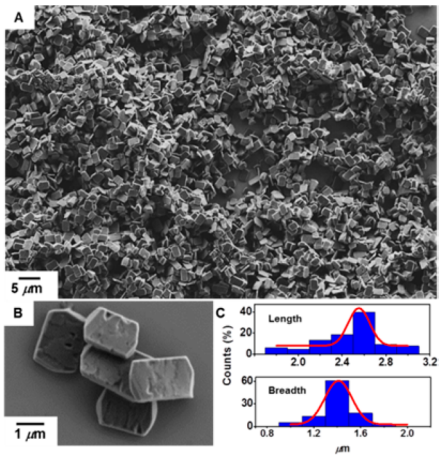

Figure 2. Morphologies of nickel chloride containing microstructures obtained by solvothermal synthesis. SEM images (A, B) of **NiClL1**. Dimensions: length: 2.6 ± 0.9 μm, width: 1.4 ± 0.5 μm, thickness: 250 ± 50 nm. (C) Histograms showing the size distribution of **NiClL1**. Reaction conditions: $NiCl_2$:**L1** = 2:1, DMF/$CHCl_3$ = 3:1 v/v, 105 °C, 5 days.

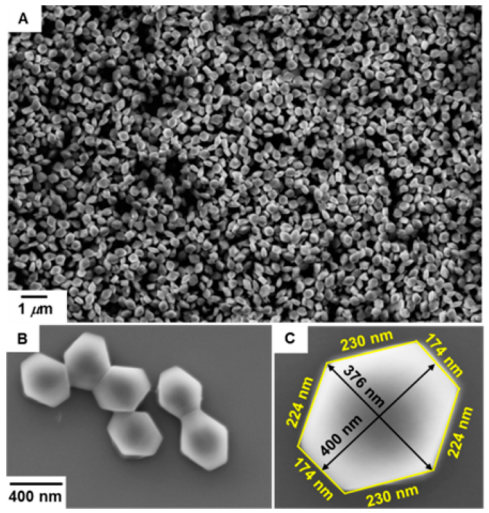

Figure 3. Morphologies of nickel bromide containing microstructures obtained by solvothermal synthesis. SEM images (A−C) of **NiBrL2**. Dimensions: diagonal: 370 ± 10 nm, side-to-side: 405 ± 10 nm, thickness: 220 ± 20 nm. Reaction conditions: $NiBr_2$:**L2** = 2:1, DMF/$CHCl_3$ = 3:1 v/v, 105 °C, 5 days.

structural differences in the organic ligand (i.e., **L1**: C≡C versus **L2**: C═C) and the anion (Cl, Br) are key factors that can be used to tune the structure of these MOFs at the (sub)microscopic level while a high level of uniformity is retained. Furthermore, the metal-to-ligand (M:L) and solvent ratios can be used to control the MOF morphology. For instance, using $NiCl_2$ and **L1** in a 1:1 ratio resulted in smaller hexagonal structures, whereas changing the chloroform content resulted in elongated structures (Figure S2). Addition of water to the reaction resulted in structural deformation (Figure S2F).

AFM measurements of **NiClL1** and **NiBrL2** confirmed the morphologies and allowed precise measurement of the structure height (Figure 4) as well as determination of mechanical properties. The elastic modulus of **NiClL1** measured by AFM nanoindentation is 5−6 GPa, which is similar to values reported for organic crystals.[36] The crystalline nature of these two MOFs was unambiguously demonstrated by TEM using selected area electron diffraction (SAED, Figures 5B inset, D).

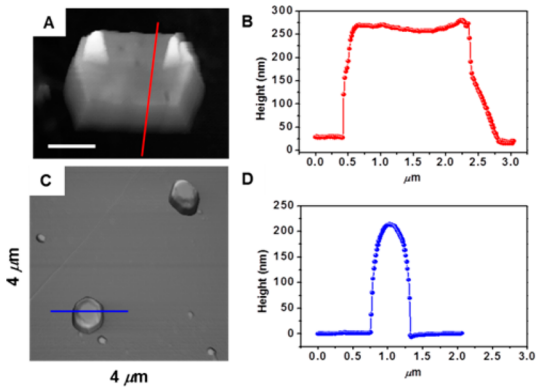

Figure 4. AFM analysis of the nickel containing microstructures. (A) AFM morphology of **NiClL1** (scale bar =1 μm). (B) Height profile corresponding to the red line in (A) of an individual crystallite. (C) AFM morphology of **NiBrL2**. (D) Height profile corresponding to the blue line in (C) of an individual crystallite.

DOI: 10.1021/ja509428a
J. Am. Chem. Soc. 2015, 137, 226−231

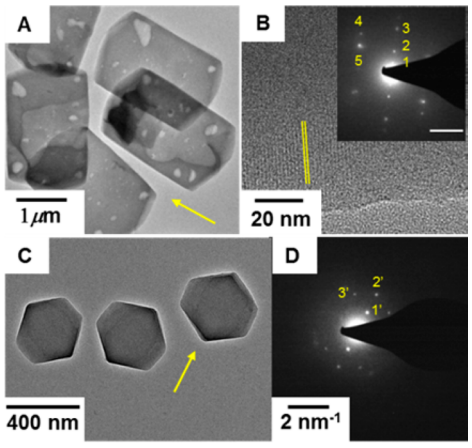

Figure 5. TEM images and SAED of the nickel containing microstructures. (A) TEM image of **NiClL1**. (B) High-magnification TEM image showing lattice planes in a single crystal of **NiClL1**, Inset: SAED pattern arising from **NiClL1**, scale bar = 2 nm^{-1}, with *d*-spacing corresponding to 1:1.79, 2:0.9, 3:0.46, 4:0.42, and 5:0.49 nm. (C) TEM image of **NiBrL2**. (D) SAED pattern arising from **NiBrL2**, with *d*-spacing corresponding to 1′:0.95, 2′:0.49, and 3′:0.55 nm. For SAED, the crystal orientation (longest axis) is indicated by the yellow arrow in (A) and (C).

XRD measurements of **NiClL1** further supported the formation of ordered structures (Figure S3A). The elemental composition of the MOFs was qualitatively confirmed by X-ray energy dispersive spectrometry (EDS), showing peaks corresponding to characteristic atoms (Figure S4).

The presence of the ligands is confirmed by FT-IR spectroscopy showing peaks corresponding to the ligand framework of **NiClL1** and **NiBrL2** that are shifted as compared to the free ligands (**L1**, **L2**; Figure S5). The molecular structures of **L1** and **L2** are unlikely to be affected by the solvothermal conditions in the presence of these nickel salts. We verified this assumption by dissolving the MOFs under strong acidic conditions (pH < 1) and subsequent isolation and characterization of the organic components. ^{1}H and $^{13}C\{^{1}H\}$ NMR spectroscopy (Figure S6) and mass-spectrometry (ESI-MS and MALDI-TOF) confirmed the ligand stability. SQUID measurements revealed paramagnetic behavior for both **NiClL1** and **NiBrL2**. The zero field cooled (ZFC) and field cooled (FC) dependences were found to be superimposed (Figure S7). These magnetic properties are in agreement with a near tetrahedral or an octahedral coordination geometry of the metal center.[37]

The isolated **NiClL1** and **NiBrL2** are air stable at room temperature in the dark for at least one year. Immersing these MOFs in DMF or water for several months does not induce any observable change in their microstructure. Thermogravimetric analysis (TGA) of **NiClL1** and **NiBrL2** showed a relatively small weight decrease of <6% at 62−68 °C, corresponding with the loss of $CHCl_3$ (Figure S8A,B). Rapid thermal processing (RTP) of **NiClL1** and **NiBrL2** under a stream of 10% H_2/N_2 and subsequent SEM analysis indicated that the structures were preserved at 200 °C. Clear deformation for both **NiClL1** and **NiBrL2** was observed at higher temperatures (Figures S9 and S10). The structures were found to be decorated with metallic nanoparticles (ø ≈ 20 nm) at ≥400 °C. The morphological stability of **NiClL1** under vacuum is higher, indicating that the thermal stability is affected by H_2 (Figure S9, bottom).

The porosity of **NiClL1** was demonstrated by gas adsorption analysis. **NiClL1** was activated at 120 °C under high vacuum for several hours to evaluate its adsorption/release efficiency for natural gas (CH_4). The CH_4 adsorption is 7.5 ± 1 wt % at 0−20 °C and 11.7 ± 1 wt % at −78.5 °C under a pressure of 35 atm. The hysteresis between adsorption and desorption runs is negligible, confirming the microporosity and the reversibility of the CH_4 uptake (Figure S11). Gas pycnometry indicated a density of 0.687 g/cm^3. The CH_4 adsorption capacity of **NiClL1** (75 cm^3 STP/cm^3) is in the range of that of COF-10, $Cd_2(AZPY)_3NO_3$, $Co_2(4,4'\text{-}BPY)_2(NO_3)_4$, $Cu_2(PIA)_2(NO_3)_4$, and the commercially available Basolite A520.[38,39]

The use of Cu salts resulted in MOFs with strikingly differently structures. Non-uniform structured MOFs were obtained with $CuCl_2$ and **L2** (Figure S12). However, the reaction of $CuBr_2$ with **L2** resulted in the formation of two interpenetrating tetrahedra (*stella octangula*) which can be described as a 3D extension of the Star of David (**CuBrL2**; Figure 6). The reaction conditions are identical to those used for the formation of **NiClL1** and **NiBrL2** (Figures 2 and 3).

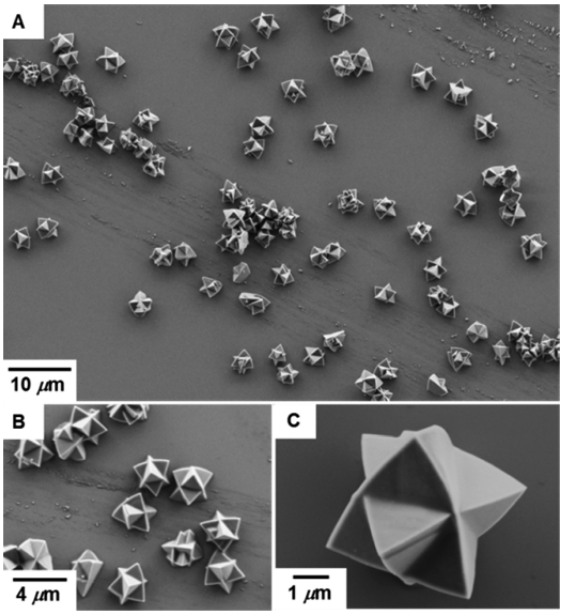

Figure 6. Interpenetrating morphologies of Cu bromide containing MOFs obtained by solvothermal synthesis. SEM images (A−C) of **CuBrL2**. Reaction conditions: $CuBr_2$:**L2** = 2:1, DMF/$CHCl_3$ = 3:1 v/v, 105 °C, 5 days.

The selection of the anions and the M:L ratio are also key parameters for the formation of well-defined Cu-based MOFs. The use of $Cu(NO_3)_2$ and a 2:1 (M:**L2**) ratio resulted in ill-defined structures, contrasted with the higher degree of uniformity obtained for a 1:1 ratio. The latter resulted in flower-like morphologies (**Cu(NO_3)L2**; Figures 7 and S13). Interestingly, performing this reaction with rigorous exclusion of air and use of dry solvents resulted in the formation of rectangular prisms with an average length of 3.65 ± 0.95 μm and breadth of 0.675 ± 0.09 μm (**Cu(NO_3)L2**$^{\#}$; Figure 8). In contrast to the other Cu-based MOFs, **Cu(NO_3)L2**$^{\#}$ does not show any evidence of interpenetration. The presence and coordination of **L2** is confirmed by FT-IR spectroscopy showing peaks corresponding to the ligand framework of **CuBrL2**, **Cu(NO_3)L2**, and (**Cu(NO_3)L2**$^{\#}$ (Figure S14). The

DOI: 10.1021/ja509428a
J. Am. Chem. Soc. 2015, 137, 226−231

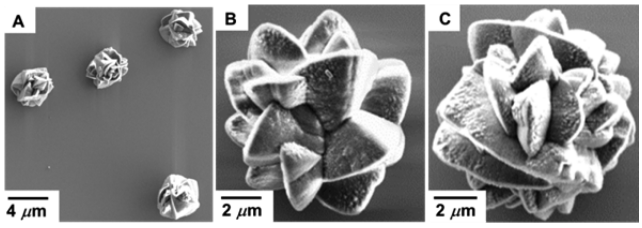

Figure 7. Interpenetrating morphologies of Cu nitrate containing MOFs obtained by solvothermal synthesis. Representative SEM images (A–C) of **Cu(NO_3)L2**. Reaction conditions: $Cu(NO_3)_2$:**L2** = 1:1, DMF/$CHCl_3$ = 3:1 v/v, 105 °C, 5 days.

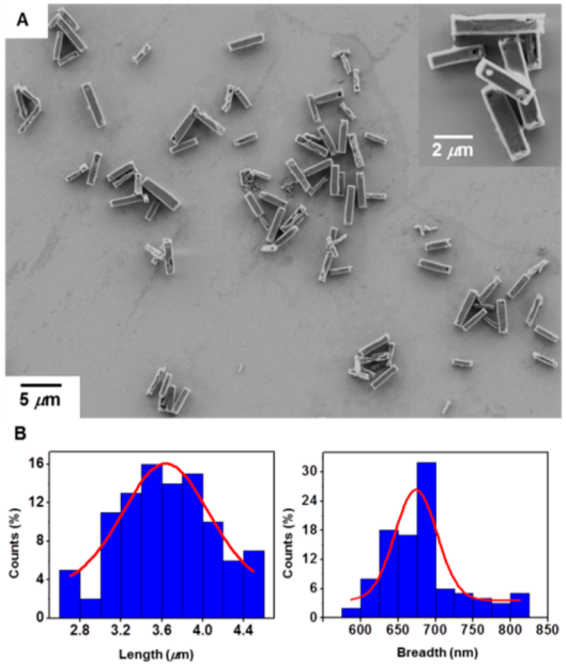

Figure 8. Rectangular morphologies of Cu nitrate containing MOFs obtained by solvothermal synthesis under inert atmosphere. Representative SEM image (A) of **Cu(NO_3)L2**#. (B) Histograms showing the size distribution of **Cu(NO_3)L2**#. Length: 3.65 ± 0.95 μm, breadth: 0.675 ± 0.09 μm. Reaction conditions (using dry solvents, under nitrogen): $Cu(NO_3)_2$:**L2** = 1:1, DMF/$CHCl_3$ = 3:1 v/v, 105 °C, 5 days.

crystalline nature of these Cu-based MOFs was unequivocally demonstrated by XRD. Powder X-ray diffraction (PXRD) patterns are shown in Figure S3C–E. The elemental composition of the MOFs was qualitatively confirmed by EDS (Figure S15). TGA showed a relatively small weight decrease of 4.5–7.4% at 61–67 °C corresponding with the loss of $CHCl_3$ (Figure S8C–E).

Dissolving the Cu-based MOFs under acidic conditions and subsequent isolation and characterization of **L2** by NMR spectroscopy and mass-spectrometry confirmed its stability (Figure S6B). The three Cu-based MOFs were found to be less uniform than **NiClL1** and **NiBrL2**, however, they still have a common structural motif. The lesser degree of uniformity for the Cu-based MOFs might be related to their higher structural complexity and larger diversity of possible structures.

The formation of the MOFs is probably a result of a complex cascade of assembly processes.[40,41] For both Ni and Cu-based MOFs, the solvent composition plays a crucial role as well for the generation of uniform structures (Figures S2, S16, and S17). Varying the DMF/$CHCl_3$ ratios and/or addition of other solvents (PhCN, DMSO, water) leads to different assemblies.

Follow-up EM studies of the formation of the Ni- and Cu-based MOFs revealed interesting mechanistic information. A time-dependent analysis showed distinctly different pathways for the formation of the uniform structures obtained. Mixing the solutions of $NiCl_2$ and $NiBr_2$ salts with the corresponding ligand (**L1** or **L2**) results in an immediate precipitation. Apparently, the process starts with the coordination of the ligand to the metal center as the first nucleation step—common in crystallizations and colloid synthesis. SEM analysis of **NiClL1** aliquots taken immediately upon mixing showed the formation of a mixture of elongated (needles) and cubical structures (<1 μm; Figure 9A). Thermolysis of this mixture

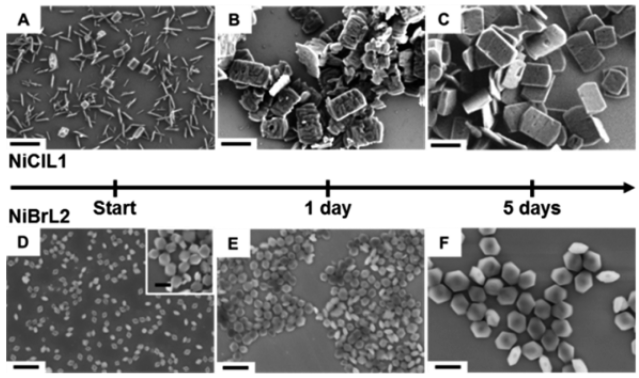

Figure 9. Time-dependent SEM analysis for the formation of Ni-based MOFs. **NiClL1**: (A) Immediately after mixing a DMF solution of $NiCl_2$ and a $CHCl_3$ solution of **L1** at room temperature. (B, C) Heating this mixture for 1 and 5 days at 105 °C, respectively. Scale bar (A–C) = 2 μm. **NiBrL2**: (D) Immediately after mixing a DMF solution of $NiBr_2$ and a $CHCl_3$ solution of **L2** at room temperature. (E, F) Heating this mixture for 1 and 5 days at 105 °C, respectively. Scale bar (D–F) = 500 nm. Inset D, scale bar = 200 nm.

resulted in the formation of premature hexagonal structures, whose overall shape and size resembles the final product, but with coarse texture and edges (Figure 9B). Continuous heating for 5 days afforded the polished **NiClL1** (Figures 2 and 9C). Amorphous infinite coordination polymers (ICP) reported by Mirkin undergo annealing similar to the structural polishing observed here.[42] The rough surfaces are likely ideal nucleation sites for the addition of more material. A different growth process operates for the formation of **NiBrL2**. In the initial stages of mixing, small and uniform crystallites (≈55 × 27 nm) are formed having the same morphology as the final product (**NiBrL2**; Figures 9D and 3). During the reaction, their size increases by almost 5-fold (Figures 9D–F). For both the Ni-based MOFs, higher temperatures and pressures increase the average size of the nanostructures and decrease the number of smaller nanostructures. The higher surface energies of smaller structures can facilitate their dissolution generating new nuclei.[43] Unlike the observed polishing process with **NiClL1**, for **NiBrL2** a different mechanism is operating that involves regular crystal growth by addition of material to the nuclei with retention of the same basic shape over the course of formation (akin to Ostwald ripening).

The time-dependent SEM analysis of the growth of the Cu-MOFs revealed a rather complicated sequence involving several intermediate structures. Mixing a solution of $CuBr_2$ with **L2** resulted at room temperature in non-uniform plate-like

DOI: 10.1021/ja509428a
J. Am. Chem. Soc. 2015, 137, 226–231

structures (Figure 10A) which transform into laterally fused spheres upon heating after 1.5 days (diameter = 650 ± 50 nm,

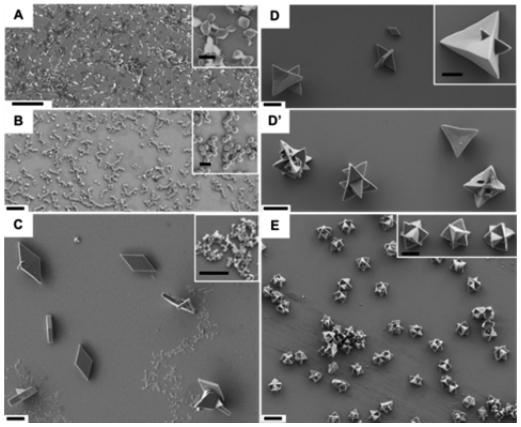

Figure 10. Time-dependent SEM analysis for the formation of **CuBrL2**. Morphologies of **CuBrL2** (A–E; scale bar = 5 μm) obtained after: (A) Immediately after mixing a DMF solution of $CuBr_2$ and a $CHCl_3$ solution of **L2** at room temperature. Inset scale bar = 200 nm. (B) Heating this mixture for 1.5 days at 105 °C. Inset scale bar = 2 μm. (C) Heating the mixture for 2.5 days at 105 °C. Inset scale bar = 1 μm. (D, D′) Heating the mixture for 3.5 days at 105 °C. Inset scale bar = 2 μm. (E) Heating the mixture for 5 days at 105 °C. Inset scale bar = 2 μm.

Figure 10B). Upon continuous heating, much larger diamond-like structures (Figure 10C) and fused structures thereof were observed. Some spherical structures remained, albeit smaller (Figure 10C, inset). Interestingly, after 3.5 days mostly pyramidal structures were present, most likely formed from a combination of fusion and nucleation (Figure 10D,D′). The inset of Figure 10D clearly shows a penetrating twin-type structure. The initial pyramidal shapes are formed by fusion of the diamond-like structures (Figures 10C,D), and their facets subsequently act as nucleation sites to afford the kinetically complex products seen in Figure 10D′. Further heating results in the thermodynamically robust **CuBrL2** (Figures 6 and 10E) that have the appearance of twinned crystals.

The formation of **Cu(NO_3)L2** starts with the formation of non-uniform plate-like structures similar to the ones observed for **CuBrL2** (Figure 11A inset). After heating for 1 day, irregular rectangular prisms were formed (Figure 11A) that transform after 2.5 days into interpenetrated structures (Figure 11B). Upon continued heating, these apparent threaded systems undergo another fusion process to provide the flower-like morphology (Figures 11C,D).

CONCLUSIONS

Our observations show that the formation of metal–organic microcrystals with a uniform size distribution can be readily achieved by solvothermal synthesis without the use of additional reagents. Others have been using solvothermal approaches for attaining structural modifications mainly at the molecular level.[15] In addition, crystal packing variation through systematic chemical modifications is known for many organic and other materials.[15,44−47] However, such an approach to obtain uniform microcrystals is rare.[5,48]

We have shown the scope of our findings using two independent approaches. Thus, we have shown that identical initial composition of the metal and ligand, but different

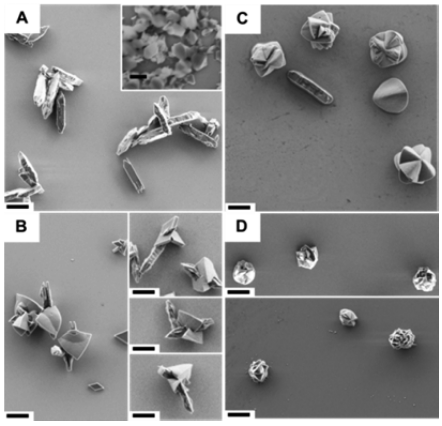

Figure 11. Time-dependent SEM analysis for the formation of **Cu(NO_3)L2**. Morphologies of **Cu(NO_3)L2** (A–D; scale bar = 5 μm) obtained after: (A) Heating a DMF solution of $Cu(NO_3)_2$ and a $CHCl_3$ solution of **L2** for 1 day at 105 °C. Inset: immediately after mixing $Cu(NO_3)_2$ and **L2**. Inset scale bar = 200 nm. (B) Heating the mixture for 2.5 days at 105 °C. (C) Heating the mixture for 3.5 days at 105 °C. (D) Heating the mixture for 5 days at 105 °C.

reaction conditions; including solvent ratios, reaction time, and an/aerobic conditions, leads to different MOF morphologies. On the other hand, structural diversity was shown under identical reaction conditions but different initial composition of metal and ligand. It is remarkable that varying the intramolecular structure (i.e., C≡C vs C═C, Cl vs Br, Ni vs Cu) has such a striking effect on the formation and uniformity of the MOFs reported here. Our approach to obtain uniformity at the (sub)micron level is sensitive to the position of the metal in the periodic table. For example, we have shown previously that the reaction of Pd(II) salts with **L2** resulted in the formation of coordination-polymer nanotubes.[35] Structural features and dimensions of such nanotubes are assembly dependent as shown by Aida et al.[49] In the present study, mixtures of (sub)microstructures were observed initially which gradually transformed into the homogeneously structured crystals. Although this work does not reveal the factors which predetermine the morphology at the molecular level because of their (sub)micron-dimensions, the possibility of custom-designed morphology is enticing. Moreover, it offers an alternative to procedures that use surfactants or external modulators.

ASSOCIATED CONTENT

Supporting Information

Experimental methods and additional characterization data, SEM images, XRD patterns, NMR and IR spectra, RTP images, EDX spectra, magnetic measurements, TGA curves, and methane adsorption isotherms. This material is available free of charge via the Internet at http://pubs.acs.org.

AUTHOR INFORMATION

Corresponding Author

milko.vanderboom@weizmann.ac.il

Notes

The authors declare no competing financial interest.

ACKNOWLEDGMENTS

We thank Dr. G. Leitus for the magnetic measurements; Dr. Y. Feldman for the XRD analyses; and Dr. S. P. Mathew for

DOI: 10.1021/ja509428a
J. Am. Chem. Soc. 2015, 137, 226–231

discussions about the magnetic measurements. This work was supported by the Minerva Foundation, the Israel Science Foundation (ISF), the Helen and Martin Kimmel Center for Molecular Design, the Alternative Sustainable Energy Research Initiative (AERI), and FP7-PEOPLE-2010-ITN (DYNAMOL). M.B. is the incumbent of the Bruce A. Pearlman Professorial Chair in Synthetic Organic Chemistry.

REFERENCES

(1) Tuxen, A.; Carenco, S.; Chintapalli, M.; Chuang, C.-H.; Escudero, C.; Pach, E.; Jiang, P.; Borondics, F.; Beberwyck, B.; Alivisatos, A. P.; Thornton, G.; Pong, W.-F.; Guo, J.; Perez, R.; Besenbacher, F.; Salmeron, M. *J. Am. Chem. Soc.* **2013**, *135*, 2273.
(2) Noorduin, W.; Grinthal, A.; Mahadevan, L.; Aizenberg, J. *Science* **2013**, *340*, 832.
(3) Pevzner, A.; Engel, Y.; Elnathan, R.; Tsukernik, A.; Barkay, Z.; Patolsky, F. *Nano Lett.* **2012**, *12*, 7.
(4) Whitesides, G. M.; Grzybowski, B. *Science* **2002**, *295*, 2418.
(5) Masoomi, M. Y.; Morsali, A. *RSC Adv.* **2013**, *3*, 19191.
(6) Gu, X. W.; Loynachan, C. N.; Wu, Z.; Zhang, Y.-W.; Srolovitz, D. J.; Greer, J. R. *Nano Lett.* **2012**, *12*, 6385.
(7) Carné-Sánchez, A.; Imaz, I.; Stylianou, K. C.; Maspoch, D. *Chem.—Eur. J.* **2014**, *20*, 5192.
(8) Sindoro, M.; Jee, A.-Y.; Granick, S. *Chem. Commun.* **2013**, *49*, 9576.
(9) Ahnfeldt, T.; Guillou, N.; Gunzelmann, D.; Margiolaki, I.; Loiseau, T.; Ferey, G.; Senker, J.; Stock, N. *Angew. Chem., Int. Ed.* **2009**, *48*, 5163.
(10) Haouas, M.; Volkringer, C.; Loiseau, T.; Ferey, G.; Taulelle, F. *Chem. Mater.* **2012**, *24*, 2462.
(11) Long, P. P.; Wu, H. W.; Zhao, Q.; Wang, Y. X.; Dong, J. X.; Li, J. P. *Microporous Mesoporous Mater.* **2011**, *142*, 489.
(12) Furukawa, H.; Cordova, K. E.; O'Keeffe, M.; Yaghi, O. M. *Science* **2013**, *341*, 1230444.
(13) Cook, T. R.; Yang, R. Y.; Stang, P. J. *Chem. Rev.* **2013**, *113*, 734.
(14) Long, J. R.; Yaghi, O. M. *Chem. Soc. Rev.* **2009**, *38*, 1213.
(15) Stock, N.; Biswas, S. *Chem. Rev.* **2011**, *112*, 933.
(16) Sindoro, M.; Yanai, N.; Jee, A.-Y.; Granick, S. *Acc. Chem. Res.* **2014**, *47*, 459.
(17) Flügel, E. A.; Ranft, A.; Haase, F.; Lotsch, B. V. *J. Mater. Chem.* **2012**, *22*, 10119.
(18) Hu, L.; Zhang, P.; Chen, Q.; Zhong, H.; Hu, X.; Zheng, X.; Wang, Y.; Yan, N. *Cryst. Growth Des.* **2012**, *12*, 2257.
(19) Lee, S. J.; Jensen, R. A.; Malliakas, C. D.; Kanatzidis, M. G.; Hupp, J. T.; Nguyen, S. T. *J. Mater. Chem.* **2008**, *18*, 3640.
(20) Shang, W.; Kang, X.; Ning, H.; Zhang, J.; Zhang, X.; Wu, Z.; Mo, G.; Xing, X.; Han, B. *Langmuir* **2013**, *29*, 13168.
(21) Chin, J. M.; Chen, E. Y.; Menon, A. G.; Tan, H. Y.; Tzi, A.; Hor, S.; Schreyer, M. K.; Xu, J. *CrystEngComm* **2013**, *15*, 654.
(22) Umemura, A.; Diring, S.; Furukawa, S.; Uehara, H.; Tsuruoka, T.; Kitagawa, S. *J. Am. Chem. Soc.* **2011**, *133*, 15506.
(23) Gao, J.; Ye, K.; Yang, L.; Xiong, W. W.; Ye, L.; Wang, Y.; Zhang, Q. *Inorg. Chem.* **2014**, *53*, 691.
(24) Ranft, A.; Betzler, S. B.; Haase, F.; Lotsch, B. V. *CrystEngComm* **2013**, *15*, 9296.
(25) Guo, Y.-N.; Li, Y.; Zhi, B.; Zhang, D.; Liua, Y.; Huo, Q. *RSC Adv.* **2012**, *2*, 5424.
(26) Cho, W.; Lee, H. J.; Oh, M. *J. Am. Chem. Soc.* **2008**, *130*, 16943.
(27) Batten, S. R. *CrystEngComm* **2001**, *18*, 1.
(28) Schilling, C. I.; Plietzsch, O.; Nieger, M.; Muller, T.; Bräse, S. *Eur. J. Org. Chem.* **2011**, *9*, 1743.
(29) Thompson, A. M. W. C.; Hock, J.; McCleverty, J. A.; Ward, M. D. *Inorg. Chim. Acta* **1997**, *256*, 331.
(30) Lu, W.; Wei, Z.; Gu, Z.-Y.; Liu, T.-F.; Park, J.; Park, J.; Tian, J.; Zhang, M.; Zhang, Q.; Gentle, T., III; Bosch, M.; Zhou, H.-C. *Chem. Soc. Rev.* **2014**, *43*, 5561.
(31) Chen, X.-Y.; Shi, H.-Y.; Huang, R.-B.; Zheng, L.-S.; Tao, J. *Chem. Commun.* **2013**, *49*, 10977.
(32) Caputo, C. B.; Vukotic, V. N.; Sirizzotti, N. M.; Loeb, S. J. *Chem. Commun.* **2011**, *47*, 8545.
(33) Tomasik, P.; Ratajewicz, Z.; Newkome, G. R.; Strekowski, L. E. *In Chemistry of Heterocyclic Compounds: Pyridine Metal Complexes*, Part 6 ; John Wiley & Sons, Inc., Hoboken, NJ, 2008; Vol. *14*.
(34) Hasenknopf, B.; Lehn, J. M.; Baum, F. D.; D, F. *Proc. Natl. Acad. Sci. U.S.A.* **1996**, *93*, 1397.
(35) Kaminker, R.; Popovitz-Biro, R.; van der Boom, M. E. *Angew. Chem., Int. Ed.* **2010**, *50*, 3224.
(36) Roberts, R. J.; Rowe, R. C.; York, P. *Powder Technol.* **1991**, *65*, 139.
(37) Bridgeman, A. J. *Dalton Trans.* **2008**, *15*, 1989.
(38) Manson, J. A.; Veenstra, M.; Long, J. R. *Chem. Sci.* **2014**, *5*, 32.
(39) Adisa, O. O.; Cox, B. J.; Hill, J. M. *Nanoscale* **2012**, *4*, 3295.
(40) Spokoyny, A. M.; Kim, D.; Sumrein, A.; Mirkin, C. A. *Chem. Soc. Rev.* **2009**, *38*, 1218.
(41) Oh, M.; Mirkin, C. A. *Nature* **2005**, *438*, 651.
(42) Jeon, Y.-M.; Armatas, G. S.; Kim, D.; Kanatzidis, M. G.; Mirkin, C. A. *Small* **2009**, *5*, 46.
(43) Murray, C. B.; Sun, S.; Daschler, W.; Doyle, H.; Betley, T. A.; Kagen, C. R. *IBM J. Res. Dev.* **2001**, *45*, 47.
(44) Zhao, D.; Timmons, D. J.; Yuan, D.; Zhou, H.-C. *Acc. Chem. Res.* **2011**, *44*, 123.
(45) Smulders, M. M. J.; Riddell, I. A.; Browne, C.; Nitschke, J. R. *Chem. Soc. Rev.* **2013**, *42*, 1728.
(46) Wang, C.; Liu, D.; Lin, W. *J. Am. Chem. Soc.* **2013**, *135*, 13222.
(47) Shirman, T.; Lamère, J.-F.; Shimon, L. J. W.; Gupta, T.; Martin, J. M. L.; van der Boom, M. E. *Cryst. Growth Des.* **2008**, *8*, 3066.
(48) Ban, Y.; Li, Y.; Liu, X.; Peng, Y.; Yang, W. *Microporous Mesoporous Mater.* **2013**, *173*, 29.
(49) Zhang, W.; Jin, W.; Fukushima, T.; Ishii, N.; Aida, T. *Angew. Chem., Int. Ed.* **2009**, *48*, 4747.

DOI: 10.1021/ja509428a
J. Am. Chem. Soc. 2015, 137, 226−231